

Development and Fidelity Assessment of Potential Flow-based Framework for Aerodynamic Modeling of High Lift Devices

M.Usman, M.Tariq, S.Nasir U.Sajjad, F.Haider, S.Saddam, and S.Salamat

Department of Aerospace Engineering, Air University, Aerospace & Aviation Campus Kamra, Pakistan

Corresponding author: M Usman (usman@aerospace.pk)

Abstract- High lift devices play a vital role in dictating the accelerated performance of an aircraft for different flight phases such as takeoff, landing, and aerobatic maneuvers. The aerodynamic design of high lift devices for any particular aircraft is an iterative process and is achieved through extensive aerodynamic Analysis of the aircraft for various flap configurations. Computational Fluid Dynamics (CFD) and Wind tunnel testing are highly effective techniques for performing the required Analysis, yet they have high computational costs and time. To overcome this shortcoming, a robust framework based on potential flow solver (PFS) and geometry parameterization is required without compromising the fidelity of the Analysis. This research aims to develop a highly robust aerodynamic analysis framework based on the Vortex Lattice Method (VLM) coupled with Polhamus Suction Analogy and parametric modeling of high lift devices. The fidelity of the framework is validated through experimental testing and is quantified by developing a fidelity assessment matrix. It is established that the computational cost of CFD has been reduced three times with only a 10% to 20% loss in accuracy when the developed framework is used. The developed PFS framework gives results from 80% to 90%. The framework results for a reference aircraft are thoroughly compared with CFD analyses. The framework provides values that agree with corresponding CFD analyses in a fraction of the time.

Keywords-- Analytical Solver; Vortex Lattice Method (VLM); Wind-tunnel, Computational Fluid Dynamics (CFD), Potential Flow Solver (PFS), High Lift Devices (HLD), Medium Altitude Long Endurance (MALE), Unmanned Aerial Vehicle (UAV)

I. INTRODUCTION

Basic aerodynamic states that an aircraft can increase its lift by increasing the angle of attack, yet, increasing the angle of attack is not possible in certain flight phases such as takeoff and landing due to tail clearance considerations which put a limit on how many angles of attack an aircraft can achieve. Moreover, in various maneuvers, there is a need to increase $C_{L,max}$ to allow the aircraft to sustain its lift. These high lift requirements necessitate using high lift devices, such as trailing and leading-edge flaps to provide additional lift to the aircraft. This consideration makes the computation of aerodynamics with high lift devices immensely important.

The deployment of various flaps has different effects on the aerodynamic characteristics of the aircraft; for example, trailing-edge flaps increase lift by increasing the effective angle of attack, leading-edge flaps increase leading edge thrust, and decrease the drag by decreasing the effective angle of attack. However, there is a need to obtain an optimum combination of leading and trailing edge flap deflections in takeoff and landing that fulfill the lift requirements while providing minimum drag In the case of takeoff and maximum drag in the case of landing. This can only be achieved through analyzing aircraft aerodynamics with

different combinations of flap deflections and angles of attack.

Modeling and meshing an aircraft with high lift devices in CFD is difficult due to mesh orthogonality issues in the gaps between the wing and high lift devices. Moreover, it takes a lot of time for the flow field computation. Hence, CFD is not a viable option in the conceptual design phase to determine the optimum high lift device configurations. It is pertinent to note that various types of drag act on an aircraft in various regimes. Inviscid drag (lift-induced drag) contributes more to subsonic aerodynamics than viscous drag [1]. Various maneuvers, takeoff, and landing mainly occur in the low subsonic regime. Considering all of the considerations, a potential flow-based analytical tool for aerodynamics computation in various maneuvers and takeoff/landing phases with high lift devices is a reasonable approach to address the complexities with minimal time.

A python programming language-based framework is developed for the aerodynamics computation of aircraft in the subsonic regime with the effects of high lift devices. It is based on a solver which implements Vortex Lattice Method (VLM) for solving potential flow around lifting surfaces in the subsonic regime. The superposition of cambered, flat, and high lift device surfaces determines the effects of leading and trailing edge flaps. To



This work is licensed under a Creative Commons Attribution 4.0 International License, which permits unrestricted use, distribution, and reproduction in any medium, provided the original work is properly cited.

reduce the computational time for the aerodynamics computation, flaps are parametrized by developing an interface that automates Vehicle Sketch Pad (VSP) geometry with the modeled parametric flaps model. Leading edge suction effects are captured by Polhamus Suction Analogy [2]. It relates the normal force induced by the leading edge flow separation and the theoretical leading edge thrust. Leading edge curvature, a key parameter in suction analogy, is used for simulating the actual physics around the leading edge.

To estimate the leading-edge radius, a parametric model is developed by using discrete points on the leading edge. This parametric model is implemented at each section of the wing to cater for the effects of aerodynamic twists. To account for the compressibility effects in a higher subsonic regime, the solution of Prandtl Glauret equation converted into Laplace equation by Gøthert transformation, is computed by the potential flow theory [3].

II. PFS-BASED FRAMEWORK

A PFS-based framework is developed for aerodynamics computation of an aerial platform in a subsonic regime with high lift devices, leading-edge suction, and compressibility effects. Polhamus leading-edge suction analogy is used for catering to the effects of leading-edge thrust and vortex lift. The Prandtl-Glauret Compressibility correction factor is applied to account for the compressibility effects. Aerodynamic modeling equations for high lift devices have been derived and integrated with a potential flow solver (PFS). Furthermore, for geometric modeling of high lift devices (HLD), a parameterization technique have been utilized and incorporated in the framework, making the whole process of computing aerodynamics of any aircraft with HLDs robust and computationally efficient.

A. POTENTIAL FLOW SOLVER

Potential flow is characterized mainly by the irrotational and incompressible flows, governed by Laplace's equation. For subsonic compressible flows, Prandtl Glauret equation needs to be converted into Laplace's equation (linear equation) through Gøthert transformation [3]. To simulate the potential flow, there are four types of elementary flows, i.e., uniform flow, source flow, doublet flow, and vortex flow [1]. Such elementary flows give the solution to Laplace's equation.

The flow field around an aircraft out of the boundary layer is irrotational. Hence, potential flow solution is applicable in the far field. The vortex lattice method is used out of several methods to solve potential flows. It approximates a three-dimensional wing into a two-dimensional planform and ignores its thickness. The planform is discretized by chord-wise and span-wise lines along the surface to form trapezoidal panels [4], as shown in Figure 1. Elementary flow over each panel is the velocity field of a horseshoe vortex with some circulation strength. A horseshoe vortex with a bound leg along the quarter chord and trailing legs extending to infinity along the inboard and outboard chord is placed on each panel. The strength of these vortices is computed on the control points located at $\frac{3}{4}$ chord of each panel. The boundary conditions are imposed on the mean camber surface to simulate the flow and maintain flow-tangency condition using

thin-airfoil theory. The downwash velocity created by the vortex at any point in the wing plane is computed using Eq. (1). Moreover, the PG-Compressibility correction factor is incorporated in (1).

$$\left(\frac{v}{U}\right) = \frac{\beta}{4\pi} \bar{I} \Delta u c_e \quad (1)$$

where,

- v Downwash velocity
- U Free stream velocity
- β Compressibility correction factor
- \bar{I} Subsonic influence function
- Δu Longitudinal perturbation velocity difference across wing surface
- c_e Element average chord

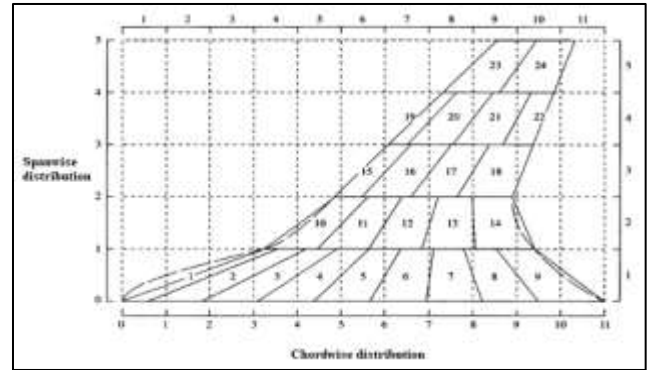


Figure 1: Wing planform discretization

The subsonic influence function of each horseshoe vortex placed on a panel is composed of three components: one represents the bound leg, and the other two represent the left and right trailing edge. The downwash at any point in the plane of the wing induced by the complete wing is found by a summation of the contribution of all individual elements. At the control point of the field element at which the flow tangency condition is met, the downwash velocity is given by (2):

$$\left(\frac{v}{U}\right)^* = \frac{\beta}{4\pi} \bar{I}^* \Delta u^* c_e^* + \frac{\beta}{4\pi} \sum \bar{I} \Delta u c_e \quad (2)$$

where * represents the field element.

Flow tangency boundary condition derived from thin airfoil theory is given by (3):

$$\left(\frac{v}{U}\right)^* = \left(\frac{dy}{dx}\right)^* \quad (3)$$

where,

- $\left(\frac{dy}{dx}\right)^*$ The slope of the mean camber at the control point

Perturbation velocity difference for field element is estimated by (4) as,

$$\Delta u^* = \frac{4\pi}{\beta} \frac{1}{I^* c_e^*} \left(\frac{dy}{dx} \right)^* - \frac{1}{I^* c_e^*} \sum \bar{I} \Delta u c_e \quad (4)$$

Perturbation velocities are converted into pressure coefficients following linearized theory assumption and are given by (5)

$$\Delta C_p^* = 2\Delta u^* \quad (5)$$

where,

ΔC_p Lifting pressure coefficient

As pressure coefficient is a linear function of perturbation velocity difference, its contribution for camber and flat wing can be added by superposition. Hence, the results from VLM based solver for other angles of attack are obtained by combining the solution of the input cambered wing ($\alpha=0^\circ$) with a resolution of a flat wing of the same platform ($\alpha=1^\circ$).

B. AERODYNAMIC MODELING OF HIGH LIFT DEVICES

Leading and trailing edge flap surfaces are represented by the same grid system as the wing. Owing to the linear nature of governing equations of the potential flow, the concept of superposition can be applied. Hence, the contribution of high lift devices is modeled by the superposition of cambered wing surface, flat wing surface, leading edge flap, and trailing edge flap. The lifting pressure coefficients for a flat and cambered wing are given in (6) and (7) correspondingly as:

$$C_p = 2 \frac{\Delta u_f \sin \alpha}{\tan 1^\circ} \quad (6)$$

$$C_p = 2\Delta u_c \quad (7)$$

The lifting pressure coefficient for leading and trailing edge flaps are given in (8) and (9) as:

$$C_p = 2 \frac{\Delta u_{le} \sin \delta_{le}}{\tan \delta_{le}} = 2\Delta u_{le} \cos \delta_{le} \quad (8)$$

$$C_p = 2 \frac{\Delta u_{te} \sin \delta_{te}}{\tan \delta_{te}} = 2\Delta u_{te} \cos \delta_{te} \quad (9)$$

The correlation of section leading edge thrust coefficient for the flat wing is given by (10)

$$C_{t,f} = \left(\frac{\sin \alpha}{\sin 1^\circ} \right)^2 \frac{\pi}{2} \frac{b}{S_{ref}} \sqrt{\tan \Lambda_{L.E}^2 + \beta^2} \times \left[(\Delta u \sqrt{x'})_{o,f} \right]^2 \quad (10)$$

where,

$C_{t,f}$ The section leading edge thrust coefficient for flat wing
 b Wing span
 S_{ref} Wing reference area
 $\Lambda_{L.E}$ Leading edge sweep angle

$(\Delta u \sqrt{x'})_{o,f}$ Leading edge singularity parameter for flat wing

The section leading edge thrust for the cambered wing is related to the thrust coefficient for the flat wing and is given as in (11)

$$C_t = C_{t,f} \left(\frac{\sin \alpha - \sin \alpha_a}{\sin 1^\circ} \right)^2 \quad (11)$$

where,

α_a Zero thrust angle of attack
 C_t The section leading edge thrust coefficient for cambered wing

Polhamus Suction analogy relates leading edge thrust coefficient with vortex force coefficient [2] as given in (12)

$$C_{vor} = \frac{C_t - C_{t,a}}{\cos \Lambda_{L.E}} \quad (12)$$

where,

$C_{t,a}$ The attainable section leading edge thrust coefficient
 C_{vor} Vortex force coefficient

The pressure coefficient is converted into section normal and axial force coefficients integrated over the wing surface and related to the angle of attack to determine the coefficient of lift and coefficient of induced drag as given by (13) and (14)

$$C_L = C_N \cos \alpha - C_A \sin \alpha \quad (13)$$

$$C_{D,i} = C_N \sin \alpha + C_A \cos \alpha \quad (14)$$

This study compares aerodynamic coefficients from a VLM-based solver to Wind Tunnel and CFD. Results of VLM, a potential flow solver, are found in close agreement with Wind Tunnel, and CFD at low to moderate (0° to 5°) angles of attack. The maximum percentage error in lift coefficient from VLM comes out to be 11% as compared to CFD in a low to moderate range of angles of attack. Wind tunnel experimentation and CFD are cost intensive in the design optimization stage. Hence, it is recommended to use VLM based solver for reasonable prediction.

C. GEOMETRIC PARAMETERIZATION OF HIGH LIFT DEVICES

A parametric model of flaps is developed to easily incorporate any changes in size and shape of flaps depending upon the requirements. Geometrical changes in flaps are required if they underperform to fulfill the requirements in an optimum way. A parametric model of flaps is developed by utilizing wing sweep angle, local chord ratios, and normalized span-wise inboard and outboard chord locations of flaps. Wing coordinates from VSP geometry are extracted in an automated way and the developed coordinate system translation algorithm is used to translate the global coordinate system of aircraft to the local coordinate system

of the wing to calculate the local chord lengths of flaps. Leading edge suction depends upon the airfoil's leading edge radius to chord ratio. Airfoil nomenclature doesn't give the airfoil's radius to chord ratio (r/c), and this parameter is also unavailable in VSP. Hence, for the automated computation of radius to chord ratio, the leading edge is modeled through discrete points, and the radius to chord ratio is computed through the parametric model.

III. FRAMEWORK VALIDATION TEST CASE

The VLM-based framework is validated against clean wings and wings with high lift devices.

A. CLEAN CONFIGURATION

The geometric features of the clean wing with diamond airfoil [5] used in this study are given in Table I. The Analysis is performed using a framework based upon an analytical solver and compared with wind tunnel data.

Table I: Geometric Specifications

Wing Span	72 in
Mean Aerodynamic chord	18.67 in
Aspect ratio	4
Taper ratio	0.5
Leading edge sweep	10°
Root chord length	24 in

B. WING WITH LEADING EDGE FLAPS

The geometrical features of leading edge flaps used in the literature [5] are given in Table II. The geometry of leading edge flaps is represented in Figure 2

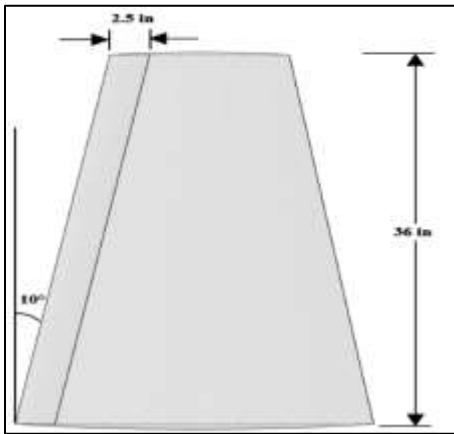


Figure 2: Leading Edge Flaps

Table II: Leading Edge Flaps Characteristics

Flaps chord to local wing chord	0.1108
Flaps inboard chord normalized location	0
Flaps outboard chord normalized location	1
Flaps deflection angle	10°

B. WING WITH TRAILING EDGE FLAPS

The geometrical features of trailing edge flaps used in the literature [5] are given in Table III. The geometry of trailing edge flaps is represented in Figure 3.

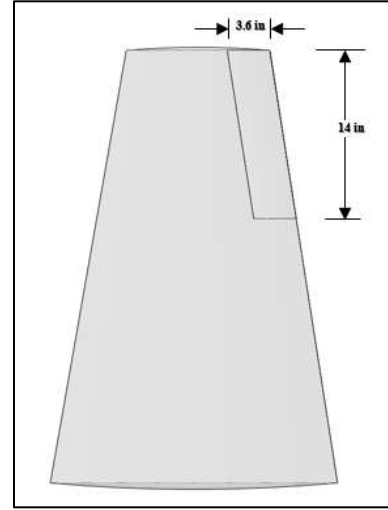


Figure 3: Trailing Edge Flaps

Table III: Trailing Edge Flaps Characteristics

Flaps chord to local wing chord	0.1479
Flaps inboard chord normalized location	0.6086
Flaps outboard chord normalized location	1
Flaps deflection angle	10°

IV. METHODOLOGY

A semi-span wing is generated using Open VSP with dimensions given in Table I and is shown in Figure 4.

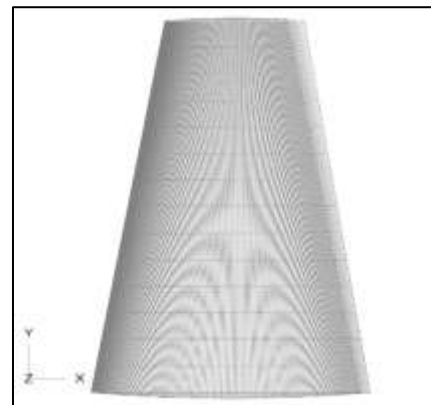


Figure 4: Open VSP Geometry for VLM Based Solver

The number of panels generated is controlled by span-wise and chord-wise distribution parameter. Wing geometry is exported from VSP in the form of coordinates and given to the solver in .txt format. The solver is executed under the abovementioned flight conditions, and an output file is generated. This file contains geometric characteristics and aerodynamic coefficients, including leading-edge thrust and vortex lift effects.

V. VALIDATION OF RESULTS

Flight conditions used in the experimental study are given in Table IV.

Table IV: Flight Conditions

Mach	0.2
Altitude	Sea-level

A. CLEAN CONFIGURATION

The results of Wind tunnel data [6] and the PFS-based framework for the coefficient of lift vs. angle of attack are plotted in Figure 5.

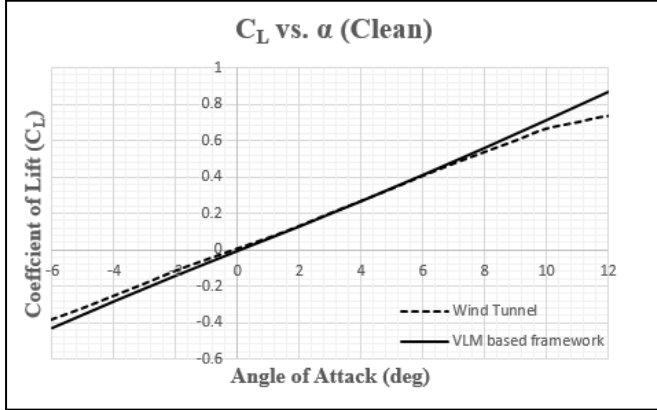


Figure 5: Comparison of Wind tunnel & VLM-based framework

The flow begins to detach at an 8-degree angle of attack from the wing, as shown in Figure 5. Therefore, VLM results tend to deviate from Wind tunnel results at an 8-degree angle of attack due to the attached flow assumption.

B. LEADING EDGE FLAPS

The results with leading edge flaps obtained from Wind tunnel data [6] and the VLM-based framework for the coefficient of lift vs. angle of attack are plotted in Figure 6.

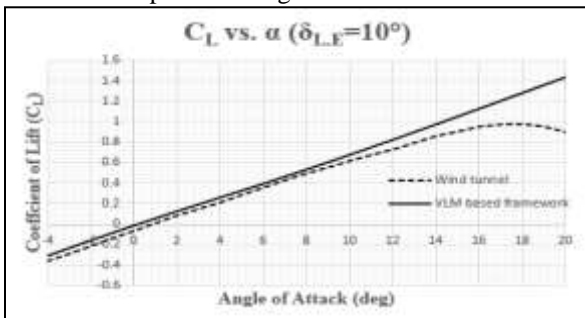


Figure 6: Comparison of Wind tunnel & VLM based framework

It is evident from the graphical representation that the results with leading edge flaps obtained from the VLM-based solver are in close agreement with the wind tunnel results.

B. TRAILING EDGE FLAPS

The effects with trailing edge flaps obtained from Wind tunnel data [6] and the VLM-based framework for the coefficient of lift vs. angle of attack are plotted in Figure 7. It is quite evident from the graphical representation that results are in close agreement

with the wind tunnel data until a 10-degree angle of attack and tend to deviate afterward due to the attached flow assumption. Therefore, it is concluded that the VLM-based framework captures the physics of high lift devices with reasonable accuracy.

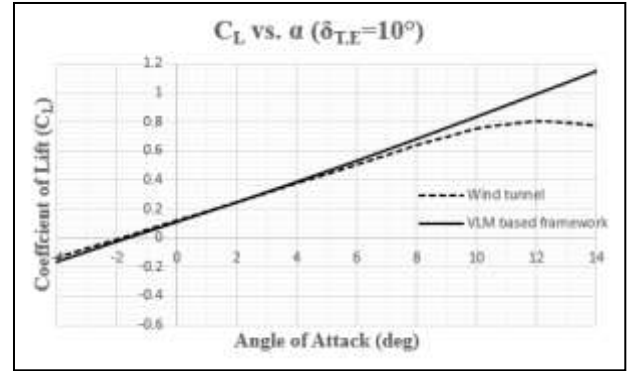


Figure 7: Comparison of Wind Tunnel & VLM Based Framework

VI. AERODYNAMIC COMPUTATION WITH HLDs FOR A MALE UAV

A Medium Altitude Long Endurance (MALE) UAV, ANKA's geometry specifications are shown in Table V [7,8]. Back and Top views of Anka UAV can be seen in Figure 8 and Figure 9. The vehicle's aerodynamics with high lift devices is computed using CFD and the PFS-based framework. The fidelity & robustness of the developed framework is determined by quantifying the computational accuracy and time for the aerodynamic Analysis. These parameters are compared with the CFD results.

Table V: Geometric specifications for Anka UAV

Parameters	Values
Wing Span	17.5 m
Length	8.6 m
Height	3.25 m
Reference Area	13.6 m ²
AR	22
C _{HT}	0.74
C _{VT}	0.016
Configuration	CVT+ATME

For the aerodynamic Analysis, the following flight conditions are employed:

Table VI: Flight Conditions

Mach	0.2
Altitude	Sea-level
Flaps deflection	0°, 25°

A. COMPUTATIONAL FLUID DYNAMICS

CFD emerged as a versatile tool over the years. It involves the discretization of the computational domain and the application of numerical schemes to solve Navier-Stokes equations. CFD analysis is performed using a commercial ANSYS fluent solver. The geometric discretization (volume mesh) around an aircraft is shown in Fig. 8.

The close-up view of surface mesh with and without flaps deflection is shown in Fig. 9. Volume mesh size that is used in this research is 13 million with the smallest element size of 0.001m and first layer height of less than 10⁻⁶.



Figure 8: Back view of Anka UAV

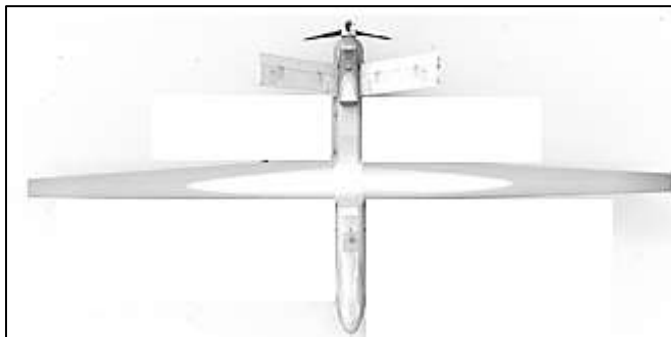


Figure 9: Top view of Anka UAV

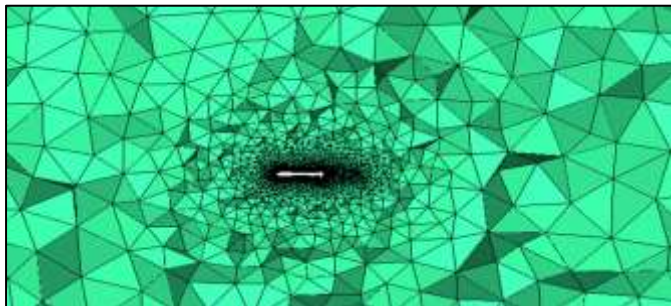


Figure 10: Volume mesh

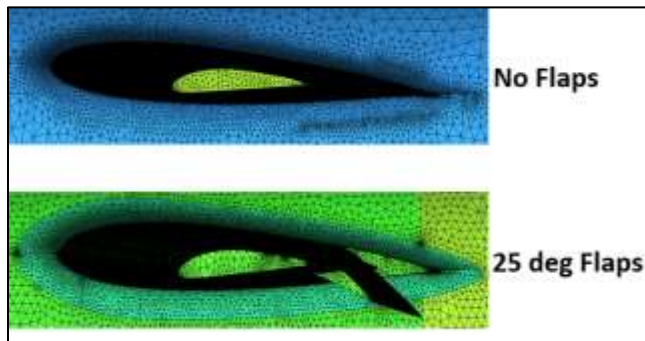


Figure 11: Surface Mesh with and without flaps

The time averaging of all the terms in Navier-Stoke's equations (known as RANS) results in turbulence stress. It needs to be modeled through turbulence models for achieving closure using

Boussinesq's hypothesis [9]. Several different turbulence models exist. Out of them, SST-K ω [10] is used which captures near wall effects as well as far field effects. The pressure contour for a wing with 25 degree flaps deflection and clean wing are shown in Fig. 10 and 11.

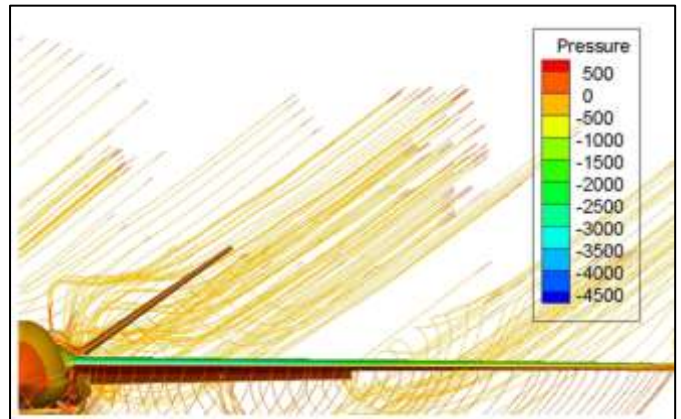


Figure 12: Pressure contour for wing with 25 degree flaps

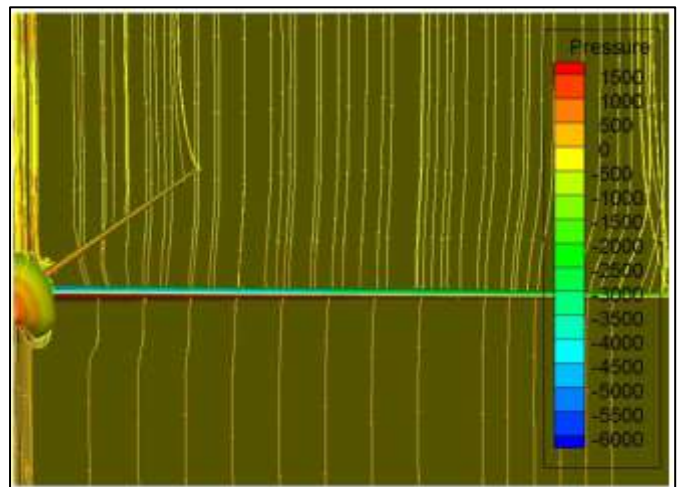


Figure 13: Pressure Contours for Clean wing

B. PFS BASED FRAMEWORK FOR AERODYNAMICS COMPUTATION WITH HLDs

A UAV geometry is generated using Open VSP. Wing-body geometry is divided along the span and chord using parameters JBYMAX and ELAR to generate the panels, as shown in Figure 14. The input file for the geometry is generated using the framework. This geometry is imported to the solver in .txt format. The solver is executed under the abovementioned flight conditions and generates an output file. This file contains the geometric characteristics and aerodynamic coefficients that incorporate the effects of leading-edge thrust and vortex lift.

The developed framework is shown in Fig. 15. It starts with the development of the Open VSP model. After the generation of the VSP model, it has to be integrated with the parametric model of flaps. The integrated VSP model is discretized into panels on which aerodynamic computation has to be carried

out. The discretized geometry is to be given to the potential flow solver. The basic potential flow solver doesn't contain any leading edge suction and flaps effects.

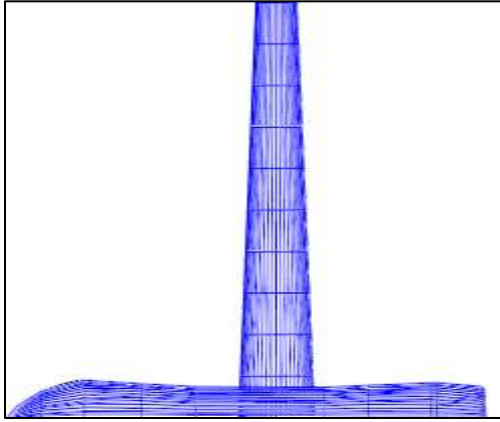


Figure 14: Panels on Open VSP geometry for VLM

It is modified in the current research, and the potential flow solver is integrated with Polhamus suction analogy's effects and flaps' aerodynamic effects. The overall framework is executed, and pressure distribution is computed based on which other aerodynamic coefficients like C_L , C_D , C_M are computed.

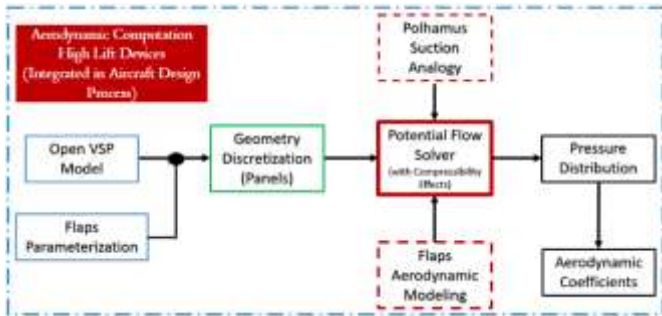


Figure 15: Developed framework for aerodynamics computation with the effects of high lift devices

VII. RESULTS AND DISCUSSION

The computational accuracy of lift and drag coefficients from the developed framework is compared with CFD results. The results are shown in Fig. 13.

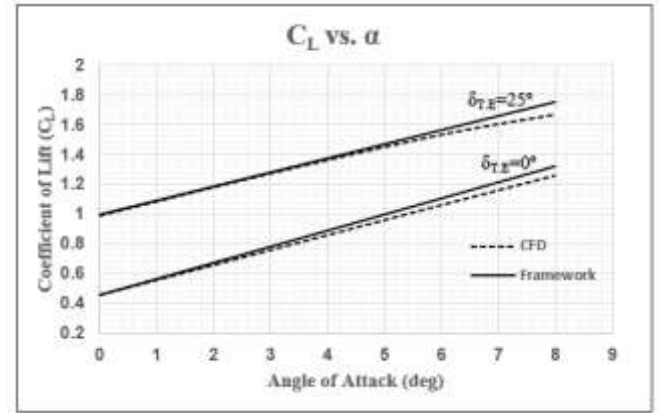


Figure 16: Comparison of CFD and Framework

Figure 16 shows that the values of lift coefficient obtained from the developed framework are in close agreement with CFD results up to an 8-degree angle of attack. Beyond this limit of attack, flow separation from the wing begins to dominate and the behavior becomes quadratic compared to linear behavior from the developed framework. Moreover, the effects of trailing edge flaps are also observable, as, with the deployment of trailing edge flaps, the overall C_L - α curve is shifted upward.

As far as the robustness of the framework is concerned, time is the major factor. Various steps involved in CFD and framework are mentioned in table 6. Out of these steps, CAD modeling, Mesh generation, and RANS-based solver are the most time-consuming steps involved in CFD. Contrary to that, the counterpart steps used in the developed framework are VSP modeling, Panels generation, and VLM-based solver. These steps reduce the overall computation time significantly. Moreover, the parametric modeling of flaps in the developed framework reduces the time involved in integrating the geometry of flaps with the comprehensive framework.

Table VII: Comparison of steps involved in CFD and PFS-based framework

Methodology	Flaps Design Parameters	VSP Modeling	CAD Modeling	Mesh Generation	Panels Generation	VLM	RANS
CFD	✓	X	✓	✓	X	X	✓
Framework	✓	✓	X	X	✓	✓	X

For a particular size and type of flap, it took around 9 days for a complete CFD simulation for a range of angles of attack. In comparison, it took around 3 days from VSP modeling until the total aerodynamic computation in the PSF-based framework. Regarding accuracy, 5% accuracy is compromised in PSF-based framework compared to CFD, and the figure goes to 10-15% for higher angles of attack. Table VII shows the fidelity assessment matrix for both methodologies.

Table VIII: Fidelity assesment matrix for CFD and PSF based framework

Fidelity Assessment Matrix		
Parameters	Computational Cost	Accuracy
CFD	3x	95%
PSF based Framework	1/3 x	80-90%

VIII. CONCLUSION

In this study, a framework based on potential flow theory is developed for the estimation of an aircraft's aerodynamic characteristics. The framework incorporates the effects of high lift devices during calculation. As with any aircraft, flaps, a common high-lift device, plays an important role during different segments of an aircraft's flight such as takeoff, landing and maneuvering, yet modelling their effects is complicated. This framework addresses the complexities and time penalties associated with modeling high lift devices using CFD solution computation. The development of a parametric model of flaps and its integration with the framework eliminates the need for flaps remodeling in VSP, saving time and computational resources in the process. The results obtained from the developed framework are validated via available wind tunnel data and CFD analyses of Anka UAVs with and without the effects of flaps. The results are in close agreement at a low to moderate angle of attack. Nevertheless, results tend to deviate at higher angles of attack due to a potential flow-based solver. Furthermore, a fidelity assessment matrix for CFD and PSF-based framework is developed, which compares both the methodologies in terms of computational cost and accuracy. It can be observed that the computational cost has been reduced by one-third when using the PSF-based framework compared to the corresponding CFD analysis with only a 10-15% compromise in accuracy. To conclude, in the early stages of the design process and to get a quick insight into the aerodynamics of aircraft with leading and trailing edge flaps, the proposed framework can save a significant amount of time and computational cost and can provide solutions that are in close agreement with high fidelity analyses such as CFD.

REFERENCES

- [1] J. D. Anderson Jr, *Fundamentals of aerodynamics*. Tata McGraw-Hill Education, 2010.
- [2] S.Nasir, et.al, "Applicability of Vortex Lattice Method and its Comparison with High Fidelity Tools" *Pakistan Journal of Engineering and Technology*, vol. 4, 2021.
- [3] W. Mason, "Applied computational aerodynamics," *Appendix D: Programs, Tuesday*, 1997.
- [4] Septiyana, A., et al. Analysis of aerodynamic characteristics using the vortex lattice method on twin tail boom unmanned aircraft. in *AIP Conference Proceedings*. 2020. AIP Publishing LLC.
- [5] B. H. Johnson Jr, "Investigation of a Thin Wing of Aspect Ratio 4 in the Ames 12-foot Pressure Wind Tunnel I: Characteristics of a Plain Wing," 1948.
- [6] J. Cho and J. Cho, "Calculation of nonlinear aerodynamic characteristics of a wing using a 3-D panel method," *International journal for numerical methods in fluids*, vol. 56, no. 1, pp. 23-35, 2008.
- [7] Seda KIRMACI ARABACI, "Aerodynamic Analysis of Anka UAV and Heron UAV", April, 2019.
- [8] Daniel Patinha Coelho, "Conceptualization and Application of Unmanned Aerial Vehicles Design Methodology", July, 2019.
- [9] Lacombe, F., D. Pelletier, and A. Garon. Compatible wall functions and adaptive remeshing for the k-omega SST model. in *AIAA Scitech 2019 Forum*. 2019.
- [10] Karansinghdangi, M.N.m., CFD Analysis of an Aircraft delta wing. *International Research Journal of Engineering and Technology (IRJET)*, vol. 03, no. 12, 2016.